

Theory, developments and applications of optical coherence tomography

P H Tomlins¹ and R K Wang²

¹ Photonics Group, National Physical Laboratory, Hampton Road, Teddington, Middlesex TW11 0LW, UK

² Cranfield Biomedical Centre, Institute of Bioscience and Technology, Cranfield University at Silsoe, Bedfordshire MK45 4DT, UK

E-mail: pete.tomlins@npl.co.uk and r.k.wang@cranfield.ac.uk

Received 15 December 2004

Published 22 July 2005

Online at stacks.iop.org/JPhysD/38/2519

Abstract

In this paper, we review the developments in optical coherence tomography (OCT) for three-dimensional non-invasive imaging. A number of different OCT techniques are discussed in some detail including time-domain, frequency-domain, full-field, quantum and Doppler OCT. A theoretical treatment is given and some relevant comparisons made between various implementations. The current and potential applications of OCT are discussed, with close attention paid to biomedical imaging and its metrological issues.

1. Introduction

In recent years, new optical imaging technologies have been developed, providing an exciting basis for investigations that span a number of scientific disciplines. The area currently attracting by far the most activity is that of biomedical imaging. This appears, in part, to be a fortunate consequence of the technological advancements made in optical telecoms, that have facilitated the mass production of an array of high specification optical devices at a relatively low cost. As a result, it has been possible to develop techniques for imaging through highly scattering materials including biological tissue. In a previous paper (Dunsby and French 2003) a number of techniques for imaging through scattering samples were reviewed. Here, we consider developments and applications of the coherence-gated imaging technique called optical coherence tomography (OCT).

OCT is an emerging non-invasive three-dimensional imaging technique, capable of producing high-resolution cross-sectional images through inhomogeneous samples, such as biological tissue. The optical configuration of OCT is that of a low coherence (white light) interferometer (LCI), similar to those used in industrial metrology for measuring the thickness of thin films (Flournoy *et al* 1972, Li *et al* 1995) and the refractive index (Maruyama *et al* 2002). The potential of LCI for three-dimensional imaging in biological tissue was first realized (Huang *et al* 1991) following its development for short range fault finding in optical fibres and photonic components

(Yougquist *et al* 1987). Since the original work, a large number of papers have been published regarding every aspect of OCT. These are available in a vast breadth of publications covering general physics, optics, materials science and a wide variety of specific medical areas such as ophthalmology, neurology and endoscopy. It is, therefore, becoming increasingly difficult to keep abreast of current developments and applications; it is perhaps even more difficult to form a comprehensive review of the subject. In this paper, a basic introduction to OCT theory is reviewed for the time, frequency, Doppler and quantum modalities. An overview of the relative optical sensitivity between time and frequency domain modalities is also given referring to papers that have recently appeared in the literature. A range of exciting applications is also reviewed to give the reader a feel for current OCT activity. Detailed aspects of OCT theory and applications not covered here have been discussed in reviews by Schmitt (1999) and Fercher *et al* (2003).

2. Optical coherence tomography

2.1. Overview

OCT is an interferometric technique, relying on interference between a split and later re-combined broadband optical field. A typical OCT schematic is shown in figure 1.

The split field travels in a reference path, reflecting from a reference mirror, and also in a sample path where it is reflected

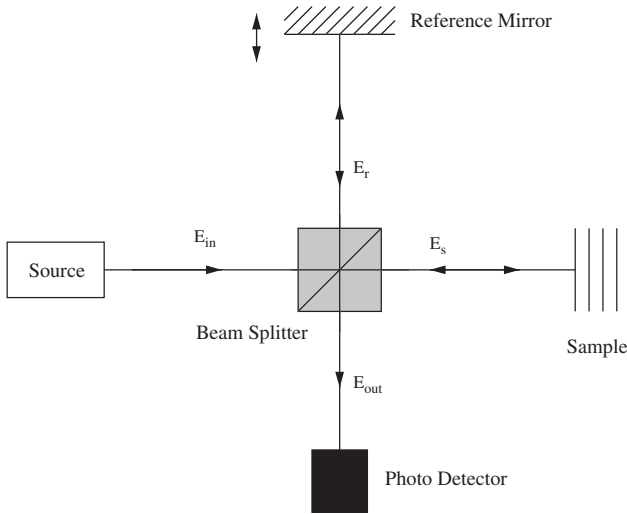


Figure 1. Basic OCT system, based on a Michelson interferometer.

from multiple layers within a sample. Due to the broadband nature of the light, interference between the optical fields is only observed when the reference and sample arm optical path lengths are matched to within the coherence length of the light. Therefore, the depth (axial) resolution of an OCT system is determined by the temporal coherence of the light source. Sharp refractive index variations between layers in the sample medium manifest themselves as corresponding intensity peaks in the interference pattern. A time domain interference pattern can be obtained by translating the reference mirror to change the reference path length and match multiple optical paths due to layer reflections within the sample. Depth information can also be derived from frequency domain measurements by Fourier transformation of the output spectrum. In such an arrangement the reference optical path length remains fixed and component frequencies of the OCT output are detected using a spectrometer.

In OCT, a two- or three-dimensional image is obtained by making multiple depth scans. These scans are performed whilst laterally scanning the beam in either one or two orthogonal directions. Typically, a two-dimensional cross-sectional image may comprise approximately 500 depth scans covering a width of 5 mm. In scattering tissue and other turbid media, the depth scan is limited primarily by optical scattering, and hence maximum reported imaging depths are between 1 and 3 mm (Brezinski and Fujimoto 1999) for a variety of tissues at wavelengths between 800 and 1300 nm.

2.2. Theoretical formulation

To describe OCT mathematically it is useful to express the electric field $E(\omega, t)$ as a complex exponential:

$$E(\omega, t) = s(\omega)\exp[-i(\omega t + kz)]. \quad (1)$$

This is a plane polarized solution to the wave-equation, with source field amplitude spectrum $s(\omega)$, frequency ω and time variation t . The second term in the exponential, in terms of wavenumber k and distance z , simply accounts for phase accumulated throughout the interferometer. Since the input

phase is arbitrary, and the interferometer only measures the relative output phase between the two optical paths, the phase term can be dropped from the input electric field. The field in each part of the interferometer is denoted by subscripts as follows; E_{in} , E_{out} , E_r and E_s , corresponding to optical fields in the input, output, reference and sample arms, respectively. The reference mirror is assumed to be ideal and the beam-splitter has reference and sample arm intensity transmittance T_r and T_s , respectively. The intensity transmission coefficients are related, such that $T_r + T_s = 1$. The sample has a frequency domain response function $H(\omega)$ that describes its internal structure and accounts for phase accumulation therein. Therefore, the component optical fields are given in terms of the input field:

$$E_{in}(\omega, t) = s(\omega)e^{-i\omega t}, \quad (2)$$

$$E_r(\omega, t, \Delta z) = (T_r T_s)^{1/2} E_{in}(\omega, t) e^{-i\phi(\Delta z)}, \quad (3)$$

$$E_s(\omega, t) = (T_r T_s)^{1/2} E_{in}(\omega, t) H(\omega), \quad (4)$$

$$E_{out}(\omega, t, \Delta z) = E_r(\omega, t) + E_s(\omega, t, \Delta z), \quad (5)$$

where $\phi(\Delta z)$ is the phase accumulated in translating the reference mirror by a geometric distance $\Delta z = \Delta t c / n_{air}$.

$$\phi(\Delta z) = \frac{2\omega n_{air} \Delta z}{c}, \quad (6)$$

Δt is the corresponding optical time of flight difference and as usual, c represents the speed of light in vacuum. n_{air} is the group refractive index of air. The factor of 2 arises because of the Michelson interferometer configuration, where the path length change is always double the distance that the reference mirror is displaced. Clearly, these equations assume that the interferometer is being operated in air. It is also noted that the frequency domain product of the sample response function and input field is equivalent to the convolution of the response function with the input field in the time domain (Hariharan 2003).

Optical detectors are square law intensity detection devices, where the recorded intensity is proportional to a time average over the electric field multiplied by its complex conjugate:

$$I(\omega, \Delta z) = \langle E_{out}(\omega, t, \Delta z) E_{out}^*(\omega, t, \Delta z) \rangle. \quad (7)$$

The angled brackets denote a time-average, given by

$$I(\omega, \Delta z) = \lim_{T \rightarrow \infty} \frac{1}{2T} \int_{-T}^T E_{out}(\omega, t, \Delta z) E_{out}^*(\omega, t, \Delta z) dt. \quad (8)$$

Substituting equation (5) into equation (7), it can be shown that the intensity is a sum of three terms:

$$I(\omega, \Delta z) = \langle E_s E_s^* \rangle + \langle E_r E_r^* \rangle + 2\Re\{\langle E_s E_r^* \rangle\}. \quad (9)$$

The first two terms can be identified as ‘self-interference’, whereas the last term is the real part (denoted \Re) of the complex ‘cross-interference’. Making the relevant substitutions from equations (2)–(4) and substituting for the field spectrum $s(\omega)$ a corresponding intensity spectrum $S(\omega) = |s(\omega)|^2$, the frequency and path difference dependent intensity is given by

$$I(\omega, \Delta z) = T_r T_s S(\omega) |H(\omega)|^2 + T_r T_s S(\omega) + 2T_r T_s \Re\{S(\omega) H(\omega) e^{-i\phi(\Delta z)}\}. \quad (10)$$

The sample response function $H(\omega)$ describes the overall reflection from all structures distributed in the z direction within the sample, and is given by

$$H(\omega) = \int_{-\infty}^{\infty} r(\omega, z) e^{i2n(\omega, z)\omega z/c} dz. \quad (11)$$

The function $r(\omega, z)$ is the backscattering co-efficient from the sample structural features, and $n(\omega, z)$ is the frequency dependent, depth varying group refractive index. The exponential term accounts for phase accumulated by the multiple optical paths within the sample.

From equation (10) it is evident that information about the optical structure of the sample can be obtained from measurements in both the time and frequency domains. These two OCT modalities, are discussed below.

2.3. Time-domain OCT

The system described above, where a reference mirror is scanned to match the optical path from reflections within the sample, is called time-domain OCT (TD-OCT). Currently, this is the most popular form of OCT arrangement. Commercial OCT instruments have been developed for ophthalmology based on the TD-OCT configuration. Equation (10) can be written as a function of reference path length displacement by integrating over the source spectrum. The expression is further simplified by assuming that the beam-splitter is lossless and has an ideal 50 : 50 split ratio, i.e. the transmissivity $T_t = T_s = 0.5$. Therefore, the TD-OCT interference pattern obtained in each axial scan is given as the sum of two terms

$$I(\Delta z) = \Gamma_0 + \Re\{\Gamma(\Delta z)\}. \quad (12)$$

Γ_0 includes only the contribution from self-interference:

$$\Gamma_0 = \frac{1}{4} \int_{-\infty}^{\infty} S(\omega) (|H(\omega)|^2 + 1) d\omega \quad (13)$$

and $\Gamma(\Delta z)$ has only a contribution from the cross interference:

$$\Gamma(\Delta z) = \frac{1}{2} \int_{-\infty}^{\infty} H(\omega) S(\omega) \cos\{\phi(\Delta z)\} d\omega. \quad (14)$$

A simple layered sample can be modelled by writing the continuous sample integral, equation (11), as a summation over N individual layers and assuming negligible dispersion:

$$H = \sum_{j=1}^N r_j \exp \left\{ i2\frac{\omega}{c} \sum_{m=1}^j n_m z_m \right\}. \quad (15)$$

Here, z_m is the thickness of the m th layer, with a group refractive index n_m . The reflectivity of each layer, r_j , can be determined by application of Fresnel's equations (Yeh 1988, Jackson 1999). Assuming that the light is perpendicular to each layer, the reflectance is

$$r_j = \frac{n_{j+1} - n_j}{n_{j+1} + n_j}. \quad (16)$$

A number of elaborate models have been developed to describe interactions of the optical field with biological tissue. These include Monte Carlo simulations based on an extended

Table 1. Theoretical sample layer properties.

Layer j	Refractive index n	Layer thickness z (μm)
1	1.00	5.00
2	1.30	15.00
3	1.50	30.00
4	1.00	0.00

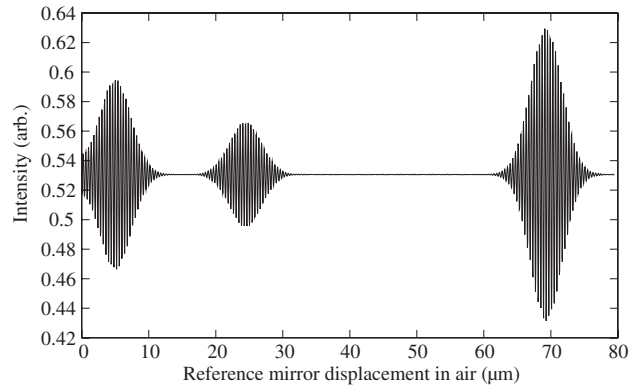


Figure 2. A TD-OCT simulation interferogram, using the layer parameters given in table 1. The source centre wavelength is 800 nm and has a Gaussian spectrum of FWHM 50 nm.

Huygens–Fresnel principle (Smithies *et al* 1998, Tycho *et al* 2002, Wang 2002a, Andersen *et al* 2004, Lu *et al* 2004) and similar analytical models (Feng *et al* 2003). A recent study has computed exact numerical solutions to Maxwell's equations for the propagation of light within scattering media (Tseng *et al* 2004). Other scattering approximations include a fractal distribution of scatterers (Wang 2000) and a photon transport model based on the Born approximation (Xu *et al* 2001).

A typical TD-OCT system might use a superluminescent diode (SLD) source operating with a centre wavelength $\lambda_0 \approx 800$ nm and spectral FWHM of around 50 nm. In such a system, the axial resolution would be approximately $6 \mu\text{m}$. Some refractive index and thickness values are given in table 1 for a theoretical layered sample.

Using these values, the resulting interferogram is plotted as a function of the reference mirror displacement, figure 2.

2.4. Fourier-domain OCT

Fourier domain OCT (FD-OCT) (Fercher *et al* 1995) has the advantage that no moving parts are required to obtain axial scans. The reference path length is fixed and the detection system is replaced with a spectrometer, figure 3. The detected intensity spectrum is then Fourier transformed into the time domain to reconstruct the depth resolved sample optical structure.

The principle of FD-OCT arises from equation (10). Since the reference mirror is now static, $\Delta z = 0$ and maintaining the assumption of an ideal 50 : 50 beam-splitter an expression for the detected frequency spectrum is obtained:

$$I(\omega) = \frac{1}{4} S(\omega) \{H(\omega) + 1\}^2. \quad (17)$$

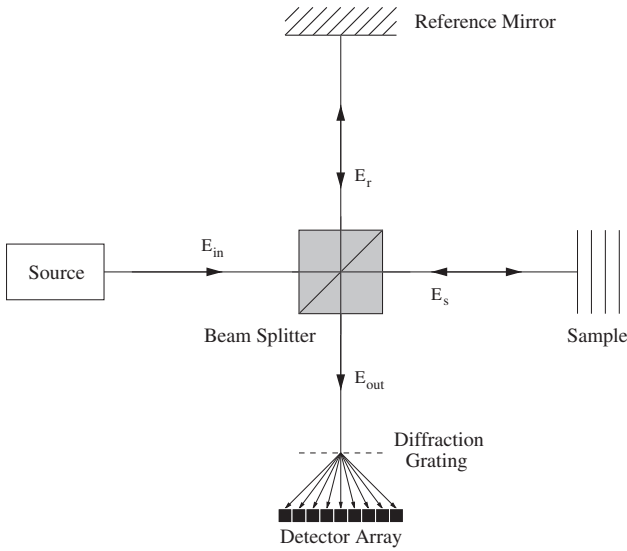


Figure 3. A FD-OCT system. The output light field is split by a diffraction grating, and component frequencies are detected by a linear detector array.

Equation (17) is useful, since it shows that an arbitrary source spectrum can be readily de-convolved from the sample response by dividing the output intensity spectrum by the measured source spectrum; a similar deconvolution technique for TD-OCT has been described previously (Wang 1999). The depth resolved structural data are obtained from the Fourier transform of $I(\omega)$ into the time domain interference pattern $I(t)$:

$$I(t) = \text{FT}\{I(\omega)\}. \quad (18)$$

FT denotes the Fourier transform operation. The interference pattern can then be displayed as a function of optical time of flight t or equivalent TD-OCT ‘reference mirror’ displacement Δz . In a real system, the output intensity spectrum $I(\omega)$ is a set of N discrete data points corresponding to an intensity measurement at each detector in the array. Therefore, the Fourier transform can be achieved by means of a fast Fourier transform (FFT) algorithm on a personal computer or in hardware. The Fourier transformed result is composed of a series of $N/2$ discrete steps in time $\Delta\tau$ determined by the detected spectral width $\Delta\Omega$:

$$\Delta\tau = \frac{2\pi}{\Delta\Omega}. \quad (19)$$

The detected spectrum can be approximated by the relation

$$\Delta\Omega = 2\pi c \frac{\Delta\lambda}{\lambda^2} \quad (20)$$

and substituted into equation (19). The conversion into the spatial domain is achieved by multiplying both sides of equation (20) by c/n_{ave} , where n_{ave} is an assumed average sample refractive index. Therefore, the maximum depth z_{max} is determined by multiplying equation (20) by the number of time domain points $N/2$ and dividing by 2 to take into account the double pass of the light through the sample:

$$z_{\text{max}} = \frac{1}{4n_{\text{ave}}} \frac{\lambda_0^2}{\Delta\lambda} N. \quad (21)$$

Hence, if a detector array consists of $N = 1024$ elements, and the source has centre wavelength $\lambda_0 = 800$ nm and bandwidth $\Delta\lambda = 50$ nm, then we find that the maximum axial scan depth for a sample with average refractive index $n_{\text{ave}} = 1.3$ must be $z_{\text{max}} \approx 2.5$ mm. Equation (21) shows that the maximum axial scanning depth scales linearly with the number of detector elements.

Because each depth scan is acquired in a single snapshot, FD-OCT has been used to acquire *in vivo* ophthalmic images (Wojtkowski *et al* 2003, Nassif *et al* 2004a, 2004b). The maximum axial scan rates that have been reported are between 15 000 and 29 000 scans per second. Parallel FD-OCT techniques have also been demonstrated that require no moving parts to capture two-dimensional depth resolved images (Zuluaga and Richards-Kortum 1999, Yasuno *et al* 2002) in real time.

The scan rate itself can be limited by the rate at which data can be transferred from the detector to a computer for processing. To achieve the maximum optical dynamic range of detection, essential for imaging through scattering tissue, it is preferable to use 12- or even 14-bit detectors. For an arbitrary bit depth b_d , each depth scan requires $b_d N$ bits of memory, where N is the number of pixels in the linear array. Assuming that a single lateral scan is generated from L_x axial scans, the memory requirement is $b_d N L_x$ bits. True video rate imaging requires 24 images per second; therefore, the required data transfer rate is $R = 24 b_d N L_x$ bits per second. For example, if a linear detector array has 1024 12-bit detectors and a single cross-sectional image is made up from $L_x = 1024$ axial scans, then the required bit rate is 302 Mbits per second, or 38 Mbytes per second. This is within the specification of USB2.0 (480 Mbps) and IEEE1394 (400 Mbps) (IEEE Std 1394 1995). To obtain video rate three-dimensional images, this figure must be multiplied by the number of lateral scans orthogonal to the cross-section L_y . If $L_y = 1024$ for the values in the previous example, then a data transfer rate of 38 Gbytes per second is required. It is currently not feasible to handle this quantity of data at such a rate using standard computer hardware and data transfer methods. One method for reducing the data transfer demands of a two-dimensional system is by using a two-dimensional CCD detector. Each line of detectors in the two-dimensional array is used to buffer each axial scan. Data can be retrieved from the CCD at some later time, removing the need to acquire data for the computer before the next axial scan can be captured.

Practically, it is straightforward to modify a TD-OCT system and convert it into a FD-OCT system. However, unlike the single analogue detector required for the time-domain modality, high dynamic range linear detector arrays, coupled with high speed data transfer electronics can be expensive. This is set to change as demand for such devices in other commercial and scientific areas increases.

FD-OCT can also be performed using a single detector by sweeping the source spectrum and detecting the intensity due to component frequencies (Chinn *et al* 1997). FD-OCT of this type has been called swept source OCT (SS-OCT), and has been demonstrated using a tunable laser. It should also be possible to use a monochromator and broadband light source; however, the spectral intensity of the monochromatic light may be too low for imaging in highly scattering media if only a single conventional SLD were used.

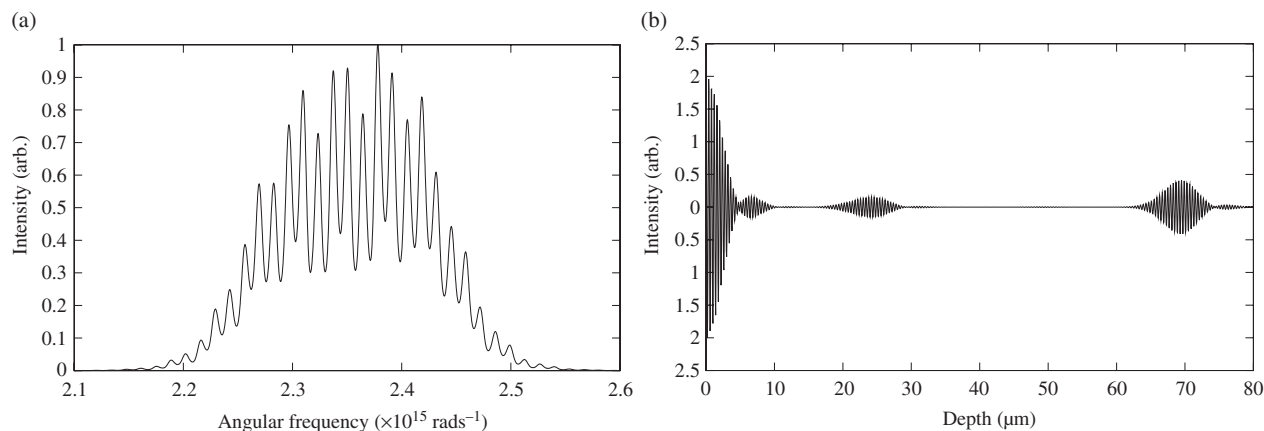


Figure 4. (a) The spectral intensity as detected at the linear detector array, or by sweeping the source frequency over the source component frequencies. (b) The Fourier transform of the spectral intensity pattern clearly shows interference occurring due to reflections at layer interfaces. This is plotted as a function of equivalent reference mirror displacement for comparison with figure 2. The interference at $\Delta z = 0$ is the Fourier transform of the source spectrum.

For comparison with the previous model of TD-OCT, the results of an FD-OCT model are shown in figures 4(a) and (b). The sample is again characterized by the parameters given in table 1. The interference at $\Delta z = 0$ in figure 4(b) is the mutual coherence function of the source.

FD-OCT is also known as spectral domain OCT (SD-OCT), frequency domain OCT and spectral radar (Lindner *et al* 2002). Throughout this paper, OCT performed in the frequency domain is referred to as FD-OCT to avoid confusion with the functional modality, spectroscopic OCT (S-OCT) that is used to perform three dimensional spectroscopy in both the time (Morgner *et al* 2000) and frequency (Leitgeb *et al* 2000) domains.

2.5. Quantum OCT

The TD-OCT and FD-OCT techniques described in the previous sections rely entirely on the classical behaviour of light. However, the quantum nature of light has led to a branch of physics, known as ‘quantum optics’. The field of quantum optics results from the development of the quantum theory of radiation (QTR) (Dirac 1927, Fermi 1932, Mandel and Wolf 1995, Loudon 2000). The classical radiation field described by Maxwell’s equations is quantized by substitution of the classical simple harmonic oscillator potential with the *quantum* harmonic oscillator potential. As a result, a number of non-classical optical phenomena have been investigated, leading to applications such as quantum cryptography and quantum optical metrology (Abouraddy *et al* 2002a, Cheung *et al* 2004). Fundamental to such fields of research is the development of quantum light sources that produce light in some known quantum state. An important example of such a source is the emission of ‘entangled photon’ states by spontaneous parametric down conversion (SPDC), both in free space using a non-linear crystal (Kwiat *et al* 1995, Lissandrin *et al* 2004) and in optical fibre (Wang *et al* 2001a, Li *et al* 2004). These have been used in probability density interference experiments, where it has been shown that the detection probability amplitudes of an entangled state interfere destructively when two paths of a suitably arranged interferometer are equal (Hong *et al* 1987). Earlier work has

also demonstrated that detection of an entangled photon rules out the existence of its entangled twin at certain other positions (Ghosh *et al* 1986, Ghosh and Mandel 1987). Here, one must be careful in the use of the term ‘photon’ since the quantum radiation field of QTR cannot be meaningfully localized, and does not behave at all like classical particles (Lamb 1995) as this expression might imply. For the sake of simplicity the photon definition of Loudon (2000) is followed, whereby a single-photon state is described by its production of a single current pulse in the ionization chamber of a photodetector. Recently, the quantum interference experiment of Hong *et al* (1987) has been extended to OCT (Abouraddy *et al* 2002b, Nasr *et al* 2003). This new modality has been called quantum OCT (QOCT) and exhibits the entirely quantum property of nonlocal dispersion cancellation (Franson 1992, Steinberg *et al* 1992). Classically, dispersion is responsible for broadening the coincidence of two light pulses propagating through media with different dispersion characteristics. In OCT this leads to the degradation of axial resolution, and normally must be compensated for by either numerical (Fercher *et al* 2001) or experimental (Smith *et al* 2002) methods. A by-product of the quantum interference of an entangled state is that a factor of two axial resolution enhancement is observed. This may prove useful as the practical axial resolution limits of classical OCT sources are approached, but only if highly efficient entangled state sources and detectors can be developed.

The experimental interferometer set-up is similar to that of Hong *et al* (1987); however, the sample is placed in one path replacing a mirror, and an optical delay line is placed in the other; figure 5.

The governing mathematics of QOCT is summarized in equation (22) and has a similar form to equation (12) for TD-OCT:

$$C(\tau) \propto \Lambda_0 - \text{Re}\{\Lambda(2\tau)\}. \quad (22)$$

The self-interference Λ_0 and cross-interference $\Lambda(\tau)$ terms are given by

$$\Lambda_0 = \int |H(\omega_0 + \Omega)|^2 S(\Omega) d\Omega \quad (23)$$

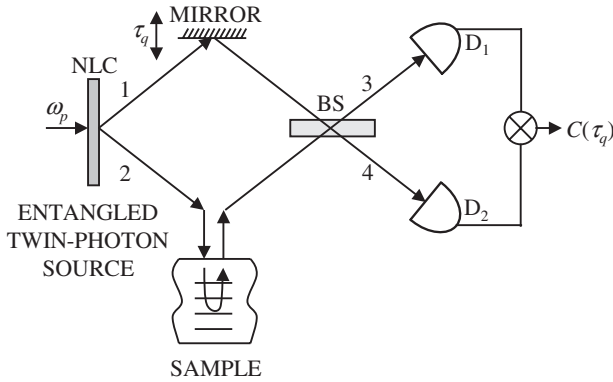


Figure 5. Experimental configuration for QOCT experiments, reproduced with kind permission from Nasr *et al* (2003).

and

$$\Lambda(\tau) = \int H(\omega_0 + \Omega)H^*(\omega_0 - \Omega)S(\Omega)e^{i\Omega\tau} d\Omega. \quad (24)$$

Here, $S(\Omega)$ describes the spectral probability amplitude where Ω is the angular frequency deviation about the central angular frequency ω_0 of the source entangled state. $H(\omega)$ is again the sample response function. These equations can be derived explicitly from QTR (Oxborrow 2004) by decomposition of the quantum field wave-packets into an infinite number of single frequency modes. Similar expressions for the joint detection probability density can be obtained by a more intuitive ‘photon-by-photon’ approach in the space-time domain (Legero *et al* 2003, Oxborrow 2003). Rigorous derivation of equations (22)–(24) requires a mathematical description of an entangled photonic state (Shih 2003) and the joint probability density function for two photons arriving simultaneously at two detectors (Glauber 1963).

Interference due to sample layer interface reflections manifests itself as a characteristic Hong–Ou–Mandel dip (Hong *et al* 1987) in the coincidence rate (figure 6).

Figure 6 demonstrates clearly, from experimental data (Nasr *et al* 2003), the factor of two enhanced resolution due to the entangled state source. The two dips correspond with the interference peaks of TD-OCT; however, a third feature midway between the dips is also apparent. This arises from interference between probability amplitudes associated with the layer reflections. It can be either a hump or a dip, depending on the layer separation. The presence of this mid-feature has more recently been used to measure the group velocity dispersion of a sample (Nasr *et al* 2004).

2.6. Full field OCT

As previously discussed, FD-OCT is a method for obtaining depth information in a single shot, without the need for mechanical scanning. In an alternative OCT method, called full field OCT (FF-OCT), a CCD camera is placed at the output in place of the TD-OCT single detector as shown in figure 7. The CCD enables the capture of two-dimensional *en face* images in a single exposure. Depth scanning is facilitated by scanning the reference mirror or moving the sample axially in the fashion of conventional TD-OCT.

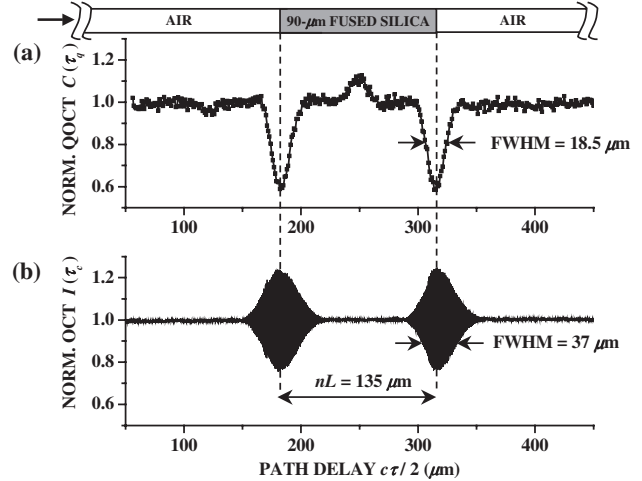


Figure 6. Hong–Ou–Mandel dips in the coincidence rate produced by QOCT scan of a 90 μm fused silica window (a). A normalized standard TD-OCT scan of the same sample demonstrates the enhanced resolution of QOCT (b). Used with permission from Nasr *et al* (2003).

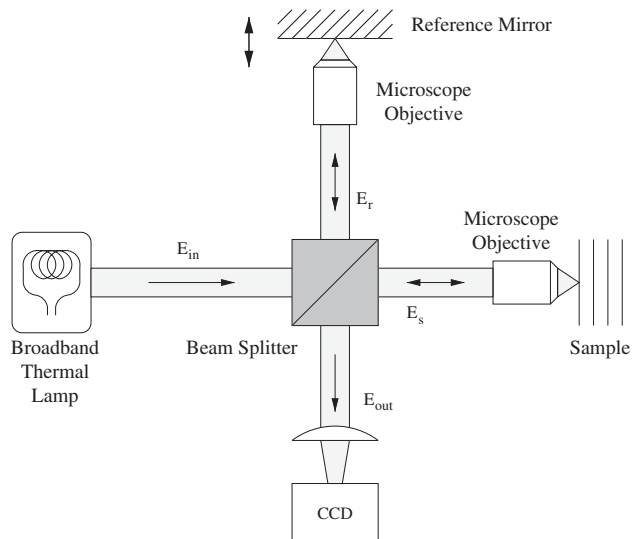


Figure 7. Experimental set-up for thermal-light full field OCT. Instead of scanning the sample laterally, two-dimensional data are obtained simultaneously from each layer by the CCD. Time-domain reference mirror scanning acts as an axial probe.

The first FF-OCT system was implemented in a commercial microscope body, using an infrared LED light source (Beaurepaire *et al* 1998). Lateral resolution was published as 2 μm , limited by the optics and camera pixel size. The axial scan resolution within the sample was approximately 8 μm , limited by the source bandwidth. More recently, this technique has been investigated using a thermal halogen light source (Vabre *et al* 2002). The use of a thermal light source has a number of advantages, it is inexpensive, has an ultra-broad spectrum ($\Delta\lambda \approx 300 \text{ nm}$) and exhibits short spatial coherence; therefore, image speckle is much reduced. The most recent results from thermal FF-OCT have reported an axial resolution of 0.7 and 0.9 μm laterally, with a three-dimensional image acquisition time of 1 s (Dubois *et al* 2004). The source was a tungsten halogen lamp centred at

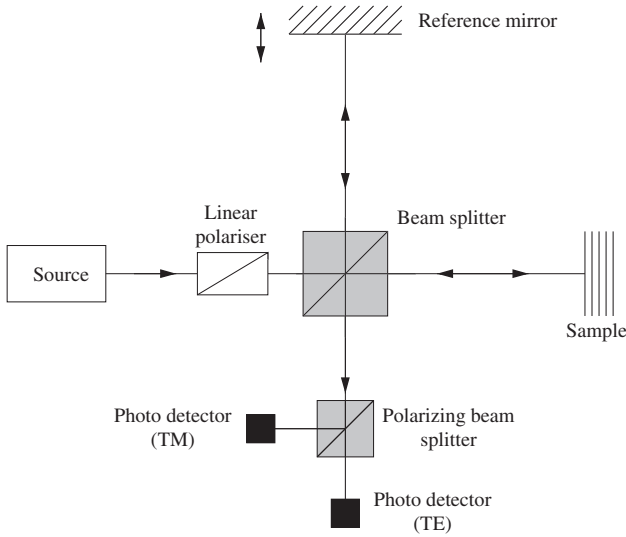


Figure 8. Experimental arrangement for polarization sensitive OCT. The polarizing beam-splitter (PBS) splits the optical output signal into its transverse electric (TE) and transverse magnetic (TM) parts.

$\lambda = 700$ nm, having a spectral FWHM $\Delta\lambda = 300$ nm; it also has a characteristically smooth spectrum that also results in a smooth temporal coherence function. This high resolution OCT modality has paved the way for three-dimensional sub-cellular real-time imaging, which is exciting for a number of areas such as developmental biology (Hoeling *et al* 2000). FF-OCT has a detection sensitivity of around 80 dB, which is lower than for conventional TD-OCT. However, this does not seem to have been a significant limiting factor in the imaging applications to which FF-OCT has so far been applied.

2.7. Polarization sensitive OCT

The TD-OCT and FD-OCT configurations do not account for birefringence within a sample, treating the electromagnetic wave as a scalar quantity. However, light waves are transverse and, therefore, have extra degrees of freedom described by the polarization state. Hee *et al* (1992) first demonstrated a low-coherence reflectometer capable of polarization sensitive measurements of birefringence. This technique was later extended by de Boer *et al* (1997) to enable two-dimensional imaging of the birefringence within a biological sample. The polarization sensitive OCT (PS-OCT) measurement apparatus is similar to that of TD-OCT or FD-OCT, with the addition of a linear polarizer after the source, and a polarizing beam-splitter (PBS) with an extra detector in the output arm (figure 8).

Propagation of light through a sample may alter the optical polarization state of the reflected light. This can occur due to optical scattering and birefringence within the sample. Birefringence describes a change in the polarization state of light due to the refractive index difference for light polarized in two orthogonal planes. Therefore, polarization sensitive measurement of the output interferogram can resolve depth correlated information about the birefringence of the sample material.

Mathematically, the two orthogonal polarization states can be treated separately as two electromagnetic waves propagating in separate interferometers. The two states are

coupled by the Jones matrix (Jerrard 1982) of the sample that specifies its birefringence.

The electric field \mathbf{E} of equation (2) is re-expressed as a vector of two orthogonal plane polarized waves, where their direction of polarization is denoted as x and y :

$$\mathbf{E}_{\text{in}} = \begin{bmatrix} s(\omega)_x e^{-i(\omega t)} \\ s(\omega)_y e^{-i(\omega t)} \end{bmatrix} = \begin{bmatrix} E_x \\ E_y \end{bmatrix}. \quad (25)$$

It follows that equations (3)–(5) translate to similar vector fields:

$$\mathbf{E}_r = (T_r T_s)^{1/2} \begin{bmatrix} E_x e^{i\phi(\Delta z)} \\ E_y e^{i\phi(\Delta z)} \end{bmatrix}, \quad (26)$$

$$\mathbf{E}_s = (T_r T_s)^{1/2} \mathbf{H} \begin{bmatrix} E_x \\ E_y \end{bmatrix}. \quad (27)$$

The output field is then described by the Jones vector

$$\mathbf{E}_{\text{out}} = \mathbf{E}_r + \mathbf{E}_s. \quad (28)$$

In equation (27) the sample response function \mathbf{H} is the Jones matrix that describes the transfer of optical energy between the two polarization states and the phase differences between the two optical axes.

Analysis of PS-OCT images is a complicated subject and has been well reviewed by de Boer *et al* (2002).

PS-OCT is attractive for medical applications, such as optical diagnosis. It provides an extra contrast mechanism that could potentially lead to optical diagnosis of certain pathologies (de Boer *et al* 1997, Mather *et al* 2004, Strasswimmer *et al* 2004).

2.8. Doppler OCT

Doppler optical coherence tomography (DOCT) (Chen *et al* 1997), also called optical doppler tomography (ODT), is based upon OCT combined with laser Doppler flowmetry (LDF). It permits the quantitative imaging of fluid flow in highly scattering media, such as monitoring *in vivo* blood flow beneath the skin (Chen *et al* 1998).

The Doppler effect describes the shift in frequency of waves reflected from moving objects. This frequency shift can be used to determine an object's velocity. For electromagnetic waves such as light, derivation of the Doppler shifted frequency from a moving object requires the application of special relativity. The result for a Doppler shifted frequency f_d is

$$f_d = \sqrt{\frac{c+u}{c-u}} f_0. \quad (29)$$

In equation (29), f_0 is the initial frequency of the electromagnetic wave, c the speed of light and u is the speed of the moving object. It is assumed that u is positive when the object is moving towards the observer. In this case, it is seen that the Doppler shifted frequency, Δf , must be greater than the initial frequency:

$$\Delta f = f_d - f_0. \quad (30)$$

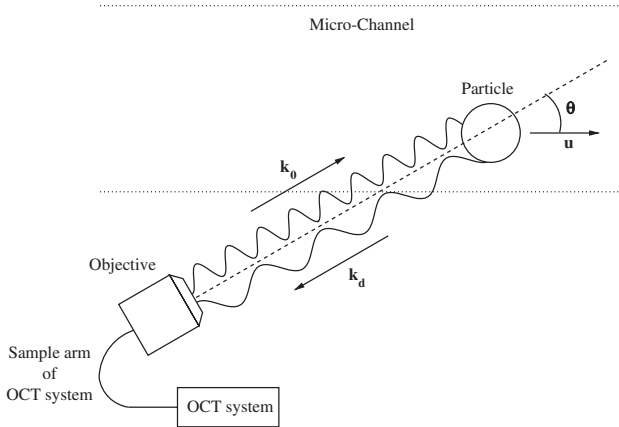


Figure 9. Schematic for the operation of optical Doppler tomography. The basic OCT system is as described in the previous sections. The sample arm is held at some angle θ to the direction of flow. Therefore, an optical signal with wave-vector k_0 falls on a particle moving with velocity u . The light scattered back into the sample objective is Doppler shifted and has wave-vector k_d .

It can be shown that when u is much less than c , the velocity of the moving sample is given by

$$\Delta f = \frac{u}{c} f_d. \quad (31)$$

In the practical DOCT system, figure 9, the interferometer sample arm is angled relative to the direction of flow by an amount θ . Detected light is scattered from a moving particle in the sample, undergoing a double Doppler shift—once from the source to the particle, and once again from the particle back to the objective. These two factors are taken into account by expressing equation (31) in terms of initial source and scattered wave-vectors k_0 and k_d , respectively. The Doppler shift can then be written as

$$\Delta f = \frac{1}{2\pi} (k_d - k_0) \cdot u. \quad (32)$$

Therefore, the velocity of moving particles can be determined from the measurement of the Doppler shift and knowledge of the relative angle between the optical signal and the flow (Chen *et al* 1999):

$$u = \lambda_0 \frac{\Delta f}{2 \cos(\theta)}. \quad (33)$$

Structural information about the sample is obtained by either conventional TD-OCT or more recently FD-OCT (Leitgeb *et al* 2004). However, to retrieve data regarding the flow of particles within a submerged capillary, extra measurements of the Doppler shifted frequency must be made. To do this in the time domain the reference mirror of the interferometer is scanned to match the path length within the capillary. At each spatial point within the capillary the detector intensity is sampled at a rate not less than two samples per time period of the source. The time varying result is then Fourier transformed to give the Doppler frequency shift due to moving particles within the capillary. By doing this at a number of points within the capillary, a profile of particle flow is determined.

The axial resolution of DOCT is again dependent on the source temporal coherence length, and the lateral scan

resolution on the beam spot size. Velocity resolution depends upon the detection electronics, scan angle and the acquisition time. Reported flow velocity resolutions are in the region $10\text{--}100 \mu\text{m s}^{-1}$; however, recent developments in Fourier domain DOCT (FD-DOCT) have shown a velocity resolution of just a few micrometres per second. FD-DOCT has also shown greater sensitivity in the region of 89–95 dB and may, therefore, lend itself to ocular flow imaging where ANSI laser safety standards require optical powers to be below 1 mW.

DOCT has been applied to a number of situations. Not least of these, imaging *in vivo* blood flow in both the skin (Zhao *et al* 2000) and retina (Leitgeb *et al* 2003b) has been demonstrated. The capability of DOCT to measure flow within a scattering sample also has potential in new areas of research such as micro-fluidics (Wang 2004).

3. Practical aspects of OCT system design

3.1. Sources and axial resolution

In OCT, it is the source that determines the general performance of the system. For example, the optical bandwidth determines the axial resolution, and the nominal wavelength determines the achievable penetration depth. In biological tissue, the OCT imaging depth is limited by both absorption and scattering. These optical properties of tissue have been investigated to some degree both experimentally (Cheong *et al* 1990, Schmitt *et al* 1994, Matcher *et al* 1997) and by a number of analytical and numerical models (Schmitt and Kumar 1998, Smithies *et al* 1998, Thrane *et al* 2000). Theoretical models have shown good agreement with experiment (Andersen *et al* 2004) and have been used successfully to extract optical scattering and attenuation information from OCT images (Thrane *et al* 2004). In non-transparent biological tissues high resolution images have been obtained at depths between 1 and 3 mm depending on the wavelength of the light source used and the opacity of the tissue investigated. A recent study has shown that the depth resolution degrading effects of dispersion in biological tissue can be significantly reduced by using a centre wavelength around $1.0 \mu\text{m}$ (Wang *et al* 2003a).

Axial (depth) resolution is an important specification of an OCT system. In many biomedical applications high axial resolutions are required to distinguish cellular boundaries and types (Boppart *et al* 1998a). In OCT related literature the system axial resolution is generally defined as half the source coherence length l_c . The coherence length can be defined in a number of ways, the most commonly quoted of these in OCT is the full-width at half-maximum (FWHM) of the source self-coherence function (SCF) multiplied by the speed of light. The SCF is simply the inverse Fourier transform of the source intensity spectrum. This and other metrics have been investigated for Gaussian and Lorentzian spectral profiles (Akçay *et al* 2002), where it was concluded that the assumption of a Gaussian spectrum may not provide a reliable prediction of the axial resolution. However, the Gaussian source approximation is convenient and well established in the OCT community; therefore it has been used here, where the Gaussian is defined in terms of its $1/e$ width w :

$$w = \frac{\Delta w}{2\sqrt{\ln 2}}. \quad (34)$$

The spectral FWHM is represented by $\Delta\omega$. The inverse Fourier transform of a Gaussian spectrum parametrized by w yields a temporal pulse whose envelope is also Gaussian, described by $A(t)$:

$$A(t) = e^{-1/4t^2w^2}. \quad (35)$$

The FWHM of $A(t)$ is called the coherence time t_c of the source, and can be derived from equation (35) as

$$t_c = \frac{1}{\Delta\nu} \frac{4 \ln(2)}{\pi}. \quad (36)$$

The frequency spectral width $\Delta\nu$ is then related to the equivalent wavelength range by the differential

$$\frac{d\nu}{d\lambda} \approx \frac{\Delta\nu}{\Delta\lambda} = -\frac{c}{\lambda^2}. \quad (37)$$

Hence, the axial resolution, in a vacuum, of an OCT system can be written as the coherence length l_c of the source. The coherence length is simply the coherence time multiplied by the speed of light, i.e. $l_c = ct_c$:

$$l_c = \frac{4 \ln(2)}{\pi} \frac{\lambda_0^2}{\Delta\lambda} \approx 0.88 \frac{\lambda_0^2}{\Delta\lambda}, \quad (38)$$

where λ_0 is the source centre wavelength, related to the source centre frequency by $\omega_0 = 2\pi c/\lambda_0$. Therefore, the OCT resolution R_{OCT} is given by

$$R_{\text{OCT}} = \frac{l_c}{2} \approx 0.44 \frac{\lambda_0^2}{\Delta\lambda}. \quad (39)$$

Following this definition, a typical SLD source having a centre wavelength $\lambda_0 = 820$ nm and spectral FWHM $\Delta\lambda = 20$ nm, has a theoretical axial resolution of approximately $15 \mu\text{m}$.

By far, the most common broadband sources used for OCT are SLDs. These devices are inexpensive and have broad spectra in the region 10–70 nm FWHM over centre wavelengths ranging from 675 to 1550 nm (Fercher *et al* 2003). They also lend themselves to OCT because of their generally Gaussian intensity spectrum. More recently, high axial resolution OCT has been demonstrated by coupling the output from two SLDs together using optical fibre couplers. The individual SLDs used had centre wavelengths of 840 and 920 nm (Ko *et al* 2004) yielding a broad FWHM output spectrum of 155 nm. The reported axial resolution was $3.0 \mu\text{m}$ in air with an output power of 4 mW. The potential of ultrahigh resolution OCT (UHR-OCT) has been demonstrated in a number of biomedical applications. Primarily, UHR-OCT images have been obtained using broadband emission generated with ultrafast laser technology in a number of different configurations. For a comprehensive review of UHR-OCT and the associated broadband sources the reader is referred to papers by Drexler (2004) and Unterhuber *et al* (2004).

At the cutting edge of broadband light generation is the Ti:Sapphire laser. These devices have been used to generate broadband light directly, demonstrating near Gaussian spectral profiles with a 176 nm FWHM and 20 mW output power (Unterhuber *et al* 2003). Hence, the achievable

axial resolution is close to $1.0 \mu\text{m}$. This system has since evolved, and is reported to have a spectral FWHM up to 260 nm enabling sub-micrometre axial resolution (Unterhuber *et al* 2004). Ti:Sapphire lasers typically have an output centre wavelength around 780 nm. A broad ‘supercontinuum’ spectrum can be generated from the self-phase modulation (SPM) of ultrashort optical pulses in photonic crystal fibres (PCFs) tailored specifically for high non-linearity. SPM of an optical pulse occurs when light of different intensity within the pulse modulates the second-order refractive index. SPM has been extensively studied in standard telecoms silica optical fibres (Agrawal 1995) and also in doped fibres used in optical amplifiers (Tomlins 2003). Doped fibre sources of amplified spontaneous emission (ASE) have been used previously in LCI for precision characterization of photonic components such as optical fibre Bragg gratings (Chapeleau *et al* 2002).

Recent results have demonstrated the use of Raman pumping to achieve a supercontinuum in PCF with a flat spectral output approximately 300 nm wide centred at 550 nm (Champert *et al* 2004). A longer wavelength broadband source candidate comes from supercontinuum generation in standard dispersion shifted optical telecoms fibres. Using stimulated Raman scattering, it has been possible to generate a spectral bandwidth of 544 nm (Abeeluck *et al* 2004). However, this source is centred at 1480 nm, which coincides with the peak water absorption wavelength.

A disadvantage of such non-Gaussian sources is that they give rise to sidelobes in the final interferogram that appear as shadow artefacts in the final image. Although these can be corrected to some degree by numerical methods (Wang 1999, Tripathi *et al* 2002), it is preferable to start with a Gaussian input spectrum. To suppress ghosting due to sidelobes, spectral shaping of the input spectrum has been successfully applied in a free-space Michelson interferometer (Akçay *et al* 2003).

3.2. Lateral resolution

One of the apparent advantages of OCT is that the lateral resolution is completely de-coupled from the axial resolution. Therefore, the optical design of the system can be optimized for lateral scanning, with no effect on the axial resolution. However, from the geometrical optical constraints of the sample arm optics it is found that by increasing the lateral resolution, maximum depth penetration is sacrificed. This can be seen by inspection of Abbé’s rule for the lateral resolution Δx (Wang *et al* 2002b):

$$\Delta x = 1.22 \frac{\lambda}{2\text{NA}_{\text{obj}}}. \quad (40)$$

NA_{obj} is the numerical aperture of the microscope objective, which is inversely proportional to the lateral resolution. Therefore, to obtain a high lateral resolution, say $1.0 \mu\text{m}$ at a wavelength $\lambda = 800$ nm, requires an objective $\text{NA}_{\text{obj}} = 0.49$. However, the depth of field Z of such an objective is then given by (Born and Wolf 1980)

$$Z = 2 \frac{\lambda n}{\text{NA}_{\text{obj}}^2}, \quad (41)$$

where n is the sample refractive index. In free space, the achievable depth of field will be approximately $6.7 \mu\text{m}$. The

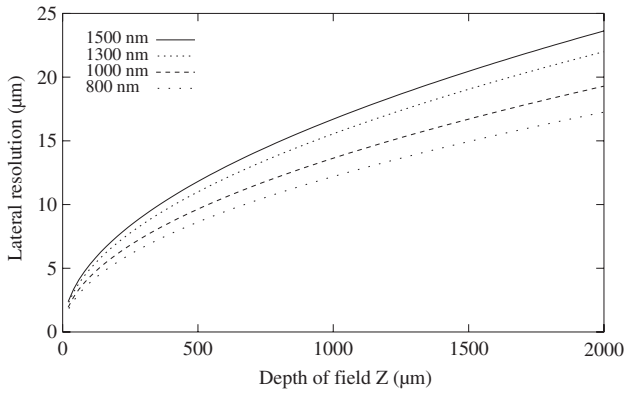


Figure 10. Lateral resolution versus depth of field for wavelengths $\lambda = 800, 1000, 1300$ and 1500 nm. Lateral resolutions $\Delta x < 5 \mu\text{m}$ limit the depth of focus significantly.

effect of the limited depth of field of high NA objectives is to reduce the detected optical signal beyond this distance, restricting the axial scan range (figure 10).

One way to compensate for this and achieve high lateral resolution and imaging depth is to incorporate some form of dynamic focusing into the sample arm optics. Such systems have been demonstrated (Schmitt *et al* 1997, Lexer *et al* 1999) and obtained high quality images over otherwise inaccessible depths.

Another approach is to produce a series of *en face* images, adjusting the focus of a high NA objective further into the sample providing a series of two-dimensional depth scans. This technique has been called optical coherence microscopy (OCM), since it incorporates the light rejection mechanism of a confocal microscope, and the coherence gating of OCT (Izatt *et al* 1994).

3.3. Optical detection sensitivity

The sensitivity of an OCT system, also called optical dynamic range, can be defined as the ratio of the signal power generated by a perfectly reflecting mirror P to the noise of the system (Fercher *et al* 2003), i.e. the power signal to noise ratio SNR_p :

$$\text{SNR}_p = \frac{i_s^2}{i_n^2}. \quad (42)$$

The signal photocurrent at the detector i_s is due to the interference term of equation (9), which, in the case of an ideal 50 : 50 beam-splitter and a perfectly reflecting sample, is equal to the total source power P . Therefore, the signal photocurrent can be written as (Leitgeb *et al* 2003a)

$$i_s = \frac{\eta q_e}{\hbar \omega_0} P, \quad (43)$$

where η the detector quantum efficiency, q_e the electron charge, \hbar is Planck's constant divided by 2π and ω_0 is the source centre angular frequency. P is the integral of the source power spectral density $S(\omega)$.

The optical detection in OCT has three significant sources of noise—shot noise, optical intensity noise and thermal noise. Shot noise describes the ‘graininess’ of low power measurements due to the quantization of the light field and

its interaction with electrons within the detector. It occurs because of the random arrival time of electrons that make up the photocurrent. The rms shot noise is expressed as (Derickson 1998, Fercher *et al* 2003)

$$i_{\text{sh}} = \sqrt{2q_e i_{\text{dc}} B}, \quad (44)$$

where i_{dc} is the dc photodetector current.

Optical intensity noise, also called relative intensity noise RIN, describes the beating between the constituent frequencies of the source spectrum. For unpolarized broadband sources such as ASE and SLDs, this turns out to be dependent only on the device spectral width (Derickson 1998):

$$i_{\text{rin}} = i_{\text{dc}} \sqrt{\frac{B}{2\pi \Delta\omega}}. \quad (45)$$

The source degree of polarization Π can also be included (Podoleanu and Jackson 1999):

$$i_{\text{rin-p}} = i_{\text{dc}} (1 + \Pi) \sqrt{\frac{B}{2\pi \Delta\omega}}. \quad (46)$$

Thermal noise (Johnson noise) is generated by an initial resistance experienced by the photocurrent in the receiver electronics. If the receiver amplifier is ideal, then this resistance is created by the detector load resistor. However, a realistic amplification process is not ideal; therefore, noise from the amplification process can also be incorporated as thermal noise by using an effective resistance R_{eff} . The thermal noise current is given by (Derickson 1998)

$$i_{\text{th}} = \sqrt{\frac{4kTB}{R_{\text{eff}}}}, \quad (47)$$

where k is Boltzmann's constant and T is the absolute temperature in Kelvin.

Each of the noise contributions is combined as a sum of squares, therefore, yielding the total noise current

$$i_n^2 = i_{\text{sh}}^2 + i_{\text{rin}}^2 + i_{\text{th}}^2. \quad (48)$$

The dc current present in equations (44), (45) and (47) is assumed to be entirely due to the reference arm optical power. In the case of an ideal 50 : 50 beam-splitter the reference arm power is equal to half the source power:

$$i_{\text{dc}} = \frac{\eta q_e P}{\hbar \omega_0 2}. \quad (49)$$

Each of the relevant expressions can be substituted into equation (42) to obtain the power SNR (Fercher *et al* 2003). However, OCT is by nature a heterodyne detection scheme optical system. Therefore, it can be arranged to achieve shot-noise limited optical detection whereby the reference arm optical field is much greater than that in the sample arm. This is often the case in OCT when imaging highly scattering and absorbing biological samples. In the shot-noise limited case the RIN and thermal noise terms in equation (48) become negligible:

$$i_n = i_{\text{sh}}. \quad (50)$$

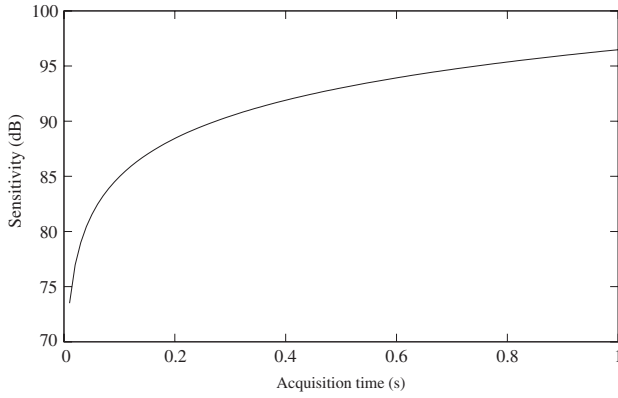


Figure 11. The shot-noise limited optical detection dynamic range of a TD-OCT system can be increased by taking longer exposures. Therefore, there is a trade-off between high speed data acquisition and high sensitivity.

It can, therefore, be shown by simple substitution that the shot-noise limited power SNR is (Yariv 1985)

$$\text{SNR}_p = \frac{\eta P}{\hbar \omega_0 B}. \quad (51)$$

Generally, in OCT, the current (or voltage) signal to noise ratio SNR_i is quoted as a figure of merit in logarithmic units. This is related to the power SNR by

$$\text{SNR}_i = 10 \log_{10} (\sqrt{\text{SNR}_p}). \quad (52)$$

The measurement bandwidth $B = 1/2\tau$ (Leitgeb *et al* 2003a) is a function of the acquisition time τ for a single photodetector measurement. It is, therefore, apparent that increasing the acquisition time improves the sensitivity of OCT but at the expense of the rate of image capture (figure 11).

4. Comparing time and Fourier domain modalities

To some extent, the choice between TD- and FD-OCT modalities may seem arbitrary, in the laboratory determined primarily by factors such as the availability of equipment. However, for specific applications there are advantages that make either one or the other preferable. FD-OCT has two main features that make it particularly attractive for a number of imaging applications. At first glance it is evident that FD-OCT requires fewer moving parts, obtaining entire depth scans in a single exposure. This fact alone implies that OCT in the Fourier domain has the potential to image equivalent samples much faster than TD-OCT. Consideration of the optical detection scheme of FD-OCT also leads to the conclusion that FD-OCT must also have a sensitivity advantage over TD-OCT.

This sensitivity advantage has been investigated theoretically and experimentally in both the FD-OCT and SS-OCT configurations (Choma *et al* 2003, de Boer *et al* 2003, Leitgeb *et al* 2003a).

In FD-OCT an array of M equivalent detectors is used to detect the light. It can be shown that the mean frequency domain noise current i_n transforms into the time domain noise current \tilde{i}_n as

$$\tilde{i}_n^2 = 2 \frac{i_n^2}{M}, \quad (53)$$

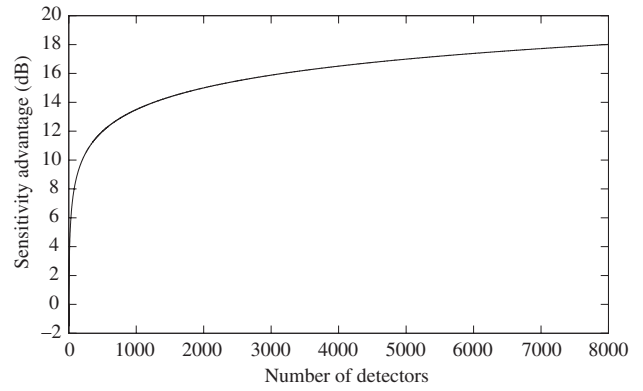


Figure 12. Sensitivity advantage of FD-OCT over TD-OCT.

where the factor of two in the numerator arises from the $M/2$ data points returned by the FFT algorithm. Assuming a Gaussian source, the signal peak detected due to a perfectly reflecting sample and reference mirror transforms into the time domain as the total optical input power P :

$$|\text{FT}\{S(\omega)\}|_{\text{peak}} = P, \quad (54)$$

where FT denotes the Fourier transform operation. The Fourier domain signal current, \tilde{i}_s , is then defined by

$$\tilde{i}_s^2 = \frac{\eta q e}{\hbar \omega_0} P. \quad (55)$$

The FD-OCT power sensitivity $\text{SNR}_{\text{fdoct}}^{(p)}$ is then written in the form of equation (42) for the TD-OCT sensitivity:

$$\text{SNR}_{\text{fdoct}}^{(p)} = \frac{\tilde{i}_s^2}{\tilde{i}_n^2}. \quad (56)$$

Therefore, it can be shown that the power SNR scales linearly with M , and hence the increased sensitivity of FD-OCT over TD-OCT (figure 12). The number of detectors is typically $M \geq 1024$ for FD-OCT:

$$\text{SNR}_{\text{fdoct}}^{(p)} = M \frac{\eta \tau}{\hbar \omega_0} P. \quad (57)$$

5. Current and emerging applications

5.1. Bio-medicine

The field of biomedical imaging has grown rapidly in recent years. In particular, optical biopsy has the potential to be a non-invasive alternative to traditional biopsy and histology. Histological slides are prepared from excised biopsy samples and stained with haematoxylin and eosin. The resulting histology can have sub-micrometre resolution, and is observed using a backlight and microscope. The staining process often leaves artefacts due to shrinking and stretching of the dehydrated tissue. High quality histology is therefore difficult, time consuming and expensive. OCT is attractive because it is rapid, high-resolution, non-invasive and inexpensive. It can also be used to generate repeatable three-dimensional quantitative images. Reported penetration

depths are between 1 and 3 mm, depending on the opacity of the tissue, such as skin, and the wavelength of light used. Further image distortions can also occur due to the refractive index mismatch between air and specimen, where light waves not perpendicular to the sample surface are refracted, causing internal features to be angularly displaced. These imaging uncertainties are not dissimilar to those encountered in ultrasound, and it has been suggested that this does not significantly compromise the diagnostic power of OCT; however, this has more recently been questioned. It is noteworthy that MRI, ultrasound and histology all suffer from similar image distortions that lead to difficulty in obtaining absolute measurements. Uncalibrated distortions lead to difficulties when intercomparing experimental results, and may ultimately place limits on the surgical applications of OCT if left un-addressed. Distortions due to refraction and layer curvature were recently investigated (Podoleanu *et al* 2004) in OCT images of the cornea, lens and retina. It was shown that in all cases the resulting axial uncertainties were significant, and in some cases they exceeded the depth resolution of the source. Lateral errors were also shown to amount to several pixels. Similar analysis of other biological tissues, and highly scattering media are yet to be carried out, but should be considered important to enable the assignment of quantitative uncertainties to OCT images.

In recent years, there have been significant advances in the understanding and optical characterization of various tissues (Schmitt *et al* 1993) and tumours (Durduran *et al* 2002, Heffer and Fantini 2002). Investigations have been carried out, looking specifically at their optical properties. For example, studies of breast cancer have revealed that tumours absorb and scatter near infrared light more than the surrounding healthy tissue (Fantini *et al* 1998). Light scattering alone may not be adequate to classify lesions as either benign or malignant. However, the use of specific optical wavelengths to investigate the oxygenation of tumours has shown promising results (Grosenick *et al* 2004). Therefore, OCT may have an important role to play in this area, especially for quantitative imaging and diagnosis. The benefits of quantitative imaging become apparent when one considers that the depth of cancer invasion is directly connected to the survival prognosis for patients.

Fibre based OCT systems can be integrated into almost any piece of existing medical equipment. *In vivo* endoscopic OCT has already been realized (Tearney *et al* 1997) and has since been successfully applied to the *in vivo* imaging of human gastrointestinal, urinary and genital tracts in a number of clinical studies (Sergeev *et al* 1997, Sivak *et al* 1999). In these studies, the constituent layers of the imaged tissue were observed by OCT along with tumours; the penetration depth was reported to be between 1.2 and 1.6 mm. The OCT endoscope is beneficial since endoscopy alone is limited to subjective interpretation of qualitative images. OCT can increase the functionality, detecting the sub-surface margins of lesions and quantifying tumour volumes.

Studies of basal cell carcinoma, the most common form of skin cancer, have investigated their birefringence using PS-OCT (Strasswimmer *et al* 2004). Physically, basal cell carcinomas are characterized by the loss of normal skin structure, i.e. alteration in the synthesis of collagen fibres and

the production of mucopolysaccharides that fill gaps within the structure. These structural changes affect the optical properties of the tissue. It was shown quantitatively that within the tumour, birefringence and optical scattering were much reduced from that of healthy skin.

OCT is attractive, since it gives a simple interferometric system for creating three-dimensional images of tissue. In the short term it may be more attractive to use OCT as a rapid screening technology, leading to standard excisional biopsy rather than for absolute diagnosis itself. Previous authors have alluded to the fact that absolute cancer diagnosis by OCT would have stringent requirements on sensitivity and specificity. However, it is clear that the resolution, depth penetration and excellent contrast between healthy and cancerous tissue can provide a non-invasive, real-time optical method to detect tumour edges, and therefore help ensure total removal.

To increase the functionality of OCT, and potentially improve its sensitivity and specificity, OCT can be used as a platform onto which other imaging modalities may be added. Examples of such hybrid systems have been developed. In one study an endoscopic OCT system was equipped with a fluorescence imaging system to demonstrate surgical guidance. The fluorescence image was used to guide the OCT scanner and image cancerous lesions in rat bladders (Pan *et al* 2003). Other functional-OCT systems have incorporated two-photon-excited fluorescence microscopy (Beaurepaire *et al* 1999) and a confocal fluorescence microscopy into the OCT system (Dunkers *et al* 2003). Functional spectroscopic OCT has also been demonstrated for profiling various fluorescent microscopy contrast agents within a sample (Yang *et al* 2004a, 2004b).

Due to the low scattering found in the optical materials of the eye, OCT has been used extensively for ophthalmic imaging (Swanson *et al* 1993, Nassif *et al* 2004b, Hee *et al* 1995a), which is by far the most mature clinical application of OCT. OCT can detect subtle changes to the eye caused during the early stages of ocular disease, such as glaucoma (Ducros *et al* 2001, Bowd *et al* 2002), and by procedures like cataract surgery (Rao *et al* 2003).

OCT has been used diagnostically in two primary ways. Direct imaging of symptoms has proven successful, for example in the detection of neurosensory detachment indicating central serous chorioretinopathy. Diagnostics may also be performed using OCT for making thickness measurements of the retina, cornea and optic nerve (Schuman *et al* 1995, Bechmann *et al* 2000, 2001, Konno *et al* 2001, Wang *et al* 2002e, 2003c, Wang 2002d). Used in this way, OCT can detect subtle changes that are missed by straight forward visual inspection. Measurement of the optic nerve has already been shown to have potential for early diagnosis of glaucoma (Schuman *et al* 1995, Liu *et al* 2001). The repeatability of these measurements was demonstrated with a standard deviation of 10–20 μm and a mean thickness of approximately 140 μm . Retinal thickness can be used to assess visual function that may indicate complications such as leakage from retinal vessels (Hee *et al* 1995b). The repeatability and reproducibility of corneal thickness measurements by OCT has also been studied by Muscat *et al* (2002). OCT may potentially be used to guide laser treatment and non-invasively monitor patient performance before, during and after surgery.

Clinical OCT systems have been adapted for monitoring the anterior chamber of the eye. In this regime, OCT can differentiate between three of the corneal layers, the epithelial-Bowman layer, Descemet-endothelial layer and corneal stroma (Hoerauf and Birngruber 2002). This capability has made OCT an attractive imaging and measurement technique to aid photorefractive surgery for the correction of myopia, hyperopia and astigmatism. OCT could be used to investigate and monitor side-effects such as haze and glare. In each of the techniques used to perform corrective eye surgery, it is essential that the exact geometric corneal thickness be known. In ophthalmology this measurement is known as pachymetric analysis. OCT offers the possibility of making such thickness measurements over a two-dimensional area. In one study (Böhnke *et al* 1999) OCT was shown to have a thickness measurement precision of $1\ \mu\text{m}$ with high reproducibility. When compared to ultrasonic pachymetry, OCT results have shown a systematic underestimation of around 1% (Gillis and Zeyen 2004). OCT measurements had a standard deviation of $0.49\ \mu\text{m}$ compared with $4.71\ \mu\text{m}$ for ultrasonic pachymetry.

In order to obtain precise geometric dimensions, an accurate knowledge of the refractive index of the layers within the eye is essential. Lin *et al* (2004) have investigated this and made *in vitro* refractive index measurements of the human cornea using OCT. In their paper, the corneal refractive index is cited with values from 1.376 to 1.450, leading to a variation in thickness measurements of more than 7%. The corneal refractive index was then measured at a wavelength of $1.3\ \mu\text{m}$ as 1.389. Such uncertainty in the obtained thicknesses may have significant implications for the success of photorefractive surgery. Podoleanu *et al* (2004) have also investigated refractive index distortion and identified this as a potential problem for the diagnosis of glaucoma and macular degeneration.

In order to further the diagnostic power of OCT, Pircher *et al* (2003) have measured differential water absorption in the human cornea by imaging with two light sources, one of which is centred in the water absorption band around 1480 nm. It has been suggested that the measurement of the spatial distribution of water absorption could contribute to future diagnostics and therapeutics.

Geometric measurements are not only important in ophthalmology. Quantitative OCT has been used to evaluate the degeneration of cartilage due to osteoarthritis (Herrmann *et al* 1999). The success of recent therapeutic developments (Lozada and Altman 1999) has been difficult to monitor in humans. This is partly due to the difficulty in measuring changes in cartilage thickness with micrometre resolution. Current measurement methods involve manual tracing of the bone-cartilage borders, a time consuming process, producing results that are open to subjective interpretation. Ultrasound, computed tomography, MRI and radiography have all been demonstrated with limited success, the main drawback being the limited spatial image resolution. OCT has several apparent advantages over alternative modalities, i.e. near video rate image acquisition, resolution improvement by at least an order of magnitude and the potentially small size and low cost of a simple fibre-optic OCT scanner. Automated OCT measurements of cartilage thickness have been shown to have good

(within $30\ \mu\text{m}$) agreement with measurements made on corresponding histological samples (Rogowska *et al* 2003).

In other medical applications, OCT has been investigated for intravascular imaging, having the potential to detect the early stages of coronary artery disease (Schmitt *et al* 2004). OCT may also be a suitable tool for imaging scar formation resulting from the use of stents. There have also been studies whereby OCT was used for dental imaging (Feldchtein *et al* 1998, Otis *et al* 2000) and neural imaging for guiding microsurgical procedures (Boppart *et al* 1998b, Boppart 2003).

Aside from the more immediate medical applications of OCT, a number of published papers have shown that OCT has the potential, and is beginning to have an impact on developmental biology and cell research. For example, the ability of OCT to acquire three-dimensional datasets, has enabled researchers to display three-dimensional projections of a developing *Xenopus* tadpole heart (Boppart *et al* 1997) and monitor development of an African clawed frog nervous system (Boppart *et al* 1996). Such monitoring is essential to forward the understanding of the complex processes that occur during neural development. OCT is well suited to this application, since the morphological changes must be visualized *in vivo*, and even small perturbations can be lethal to the organism. Preliminary work has also been carried out, using fluorescence OCM to visualize the development of cells within a tissue scaffold (Dunkers *et al* 2003).

The imaging depth limitation imposed by the highly scattering nature of many biological tissues is also attracting more interest. In a novel approach, agents have been introduced into soft tissue producing an 'optical clearing' effect (Wang *et al* 2001b, 2003b, Wang and Elder 2002c). Using this approach OCT images have been obtained of tissue below the superficial skin layer (Wang *et al* 2001b) at depths of 2 mm. Work in this area promises to be important for future clinical applications.

5.2. Tissue engineering and biomaterials

The use of biomaterials for surgical implants and tissue repairs is gaining momentum. Specifically, the areas of artificial tissue and tissue engineering are emerging fields expected to grow as commercial markets at a rate of 16%–28% (Grant *et al* 2003). Tissue engineering and artificial tissue technologies have the potential to provide a supply of tissue and organs custom grown from a patient's own cells. The future of this market will be determined by two major, and not entirely independent factors. First, the processes involved in tissue growth must be made more efficient and cost effective. The live nature of tissue complicates controlled growth. For example, cells from different patients grow at different rates (Mayhew *et al* 1998). Therefore, automated, non-invasive, fast and accurate measurement systems are essential to enable online quality control of engineered tissue growth. Second, validated standard procedures and guidelines for the characterization of biomaterials must be established. This is of paramount importance in tissue engineering, where well-characterized tissue scaffolds are required to optimize the cultivation of cells, and avoid malignancy. Ultimately, characterization is key to establishing the likely *in vivo* biocompatibility of a material (Tomlins *et al* 2004).

As an inexpensive and non-invasive quantitative three-dimensional imaging technology, OCT appears to have many attributes that could be beneficial to the biomaterials sector. It has already been demonstrated for online quality monitoring of engineered tissue for surgical implantation (Mason *et al* 2004a, 2004b). Dunkers *et al* (2003) at the national institute of standards and technology (NIST) have also demonstrated a functional OCT system for imaging cellular activity within tissue scaffolds, as well as imaging the scaffold itself. In their system, functional information regarding cell activity and structural data is obtained using a combination of confocal fluorescence microscopy (CFM) and high numerical aperture OCT.

Advances are also being made in the area of tissue scaffold design, for engineering replacement cartilage. These structures have a fibrous form, designed to enable the passage of oxygen to growing cells. It is important that the structures can be dimensionally characterized and optimized for optimal cell growth (Mason *et al* 2004b). OCT presents an ideal technique for probing these complex structures.

5.3. Nanotechnology

Currently, there is a significant push to exploit so-called nanotechnologies. Included under this title are a large number of devices and techniques that operate on the micro- to nano-metre scale. One is the area of micro-fluidics, important for bio-technology and medical research. There is also an increasing requirement for precision optical components to be manufactured on this micrometre scale. In order that these technologies may be commercially exploited it is important that there is the measurement infrastructure in place to support this industry. Manufacturers must be confident that components made and characterized in one place are compatible with those from elsewhere.

Bearing these issues in mind, some advances have been made in analysing the complex flow dynamics within micro-fluidic structures, using Doppler OCT (Wang 2004). This has both industrial and biomedical applications (Proskurin *et al* 2004), since quantitative images of flow velocity in complex internal structures can provide design engineers and clinicians with critical data.

However, there appears to be some way to go with regard to the characterization of three-dimensional optical micro-structures. Although a number of techniques have been proposed and demonstrated, which may be adequate for this purpose, there seems to have been little effort to provide a traceable measurement infrastructure. OCT has clear advantages in this area, with some limited work already published demonstrating the ability of OCT to provide accurate geometrical and optical data about a structure under examination (Fukana and Yamaguchi 1996, Haruna *et al* 1998, Westphal *et al* 2002). In one example low coherence interferometry was used to characterize the surface topology of micromechanical systems (MEMS) (O'Mahony *et al* 2003). Accurate and low cost metrology of MEMS is essential for MEMS devices to make it into large-scale production.

OCT has also been demonstrated as a promising technique for reading a new generation of high capacity multi-layered digital storage media (Chinn and Swanson 1996).

6. Materials research

Within the last few years OCT has been exploited to study polymer matrix composites (PMCs) (Dunkers *et al* 1999, 2001). OCT is an attractive imaging modality because it offers a combination of high spatial resolution and penetration depth. The imaging method requires little or no physical contact, and is entirely non-destructive.

PMCs are typically used in load bearing applications, such as bridge decks and cables, or where light weight is a primary concern, i.e. in aircraft and military weaponry. Many other applications for PMCs have also been identified: these include the marine and automotive industries, bicycle frames, ski equipment, tennis rackets and many other areas where high rigidity and low weight materials are of benefit. The materials themselves consist of a polymer matrix, forming reinforcing glass or carbon fibres into some defined structure. The matrix itself contributes to load sharing between fibres, and acts as a layer of physical protection. The resulting physical properties for any PMC are governed by the matrix material, and overall structure of the fibres. The presence of defects in the final micro-structure can severely degrade the performance of a material.

Methods for non-destructive testing of such materials are of interest, because PMCs are expensive to manufacture. Non-destructive characterization methods, such as OCT, have the potential to enable precise quality control of the material structure, leading to more cost effective production.

Similar non-destructive testing and analysis has also been applied to materials other than PMCs. For example, Duncan *et al* (1988) have investigated sub-surface defects in a range of ceramics (piezoelectric lead zirconate titanate for example), and insulating paints and plastics. In the case of ceramics, destructive testing cannot be relied upon to detect defects, since such anomalies are small, and the test method can introduce more significant defects itself. The ability of OCT to 'see' through opaque insulating layers of paint or plastic, has also been applied to the *in situ* testing of wires for breaks (Duncan *et al* 1998).

7. Conclusions

OCT is a sub-micrometre resolution, non-invasive, three-dimensional imaging technique. As such, it has the potential to be an invaluable measurement and diagnostic tool in many areas. Its wide range of current applications, from medical diagnosis and surgical guidance to the characterization of polymer micro-structures and reading of multi-layered storage media, indicate that OCT will play a major role in practical scientific innovation and research in years to come. Therefore, it is essential that OCT technologies are developed further as an enabling measurement technology. OCT has the far reaching potential to be a quantitative imaging technique that could impact many, as yet, un-explored areas, and should therefore be considered a vital measurement tool. Important emerging fields already impacted by OCT are those of tissue engineering and polymer composite manufacture.

To realize true optical biopsy, and full optical diagnosis and grading of malignant tumours by OCT will require a great number of clinical trials, and solid experimental

demonstration of the robustness of the technique. To enable such developments, the measurement technique must also be quantitatively validated. In particular, the clinical potential and reliability of OCT will be greatly enhanced by validated measurements of volume, structural dimensions and flow. These stringent requirements present new and exciting challenges for optical medical metrology.

Clearly it will not be possible to fulfill all of these criteria immediately. However, as these issues are addressed, the applicability of OCT can only grow.

Acknowledgments

The authors would like to thank Dr Mark Oxborrow of the National Physical Laboratory for providing the full derivation of the QOCT equations and helpful discussion.

This work was supported by the department of trade and industry's national measurement system directorate (NMSD).

References

- Abeeluck A K, Headley C and Jørgensen C G 2004 *Opt. Lett.* **29** 2163–65
- Abouraddy A F, Toussaint K C Jr, Sergienko A V, Saleh B E A and Teich M C 2002a *J. Opt. Soc. Am. B* **19** 656–62
- Abouraddy A F, Nasr M B, Saleh B E A, Sergienko A V and Teich M C 2002b *Phys. Rev. A* **65** 053817–1
- Agrawal G P 1995 *Nonlinear Fiber Optics* 2nd edn (New York: Academic)
- Akçay A C, Rolland J P and Eichenholz J M 2003 *Opt. Lett.* **28** 1921–3
- Akçay C, Parrein P and Rolland J P 2002 *Appl. Opt.* **41** 5256–62
- Andersen P E, Thrane L, Yura H T, Tycho A, Jørgensen T M and Frosz M H 2004 *Phys. Med. Biol.* **49** 1307–27
- Beaurepaire E, Boccara A, Lebec M, Blanchot L and Saint-Jalmes H 1998 *Opt. Lett.* **23** 244–6
- Beaurepaire E, Moreaux L, Amblard F and Mertz J 1999 *Opt. Lett.* **24** 969–71
- Bechmann M, Thiel M J, Neubauer A S, Ullrich S, Ludwig K, Kenyon K R and Ulbig M W 2001 *Cornea* **20** 50–4
- Bechmann M, Thiel M J, Roesen B, Ullrich S, Ulbig M W and Ludwig K 2000 *Br. J. Ophthalmol.* **84** 1233–7
- Böhne K, Masters B R, Wliti R, Ballif J J, Chavanne P, Gianotti R and Salathé R P 1999 *J. Biomed. Opt.* **4** 152–6
- Boppart S A 2003 *Psychophysiology* **40** 529–41
- Boppart S A, Bouma B E, Pitris C, Southern J F, Brezinski M E and Fujimoto J G 1998a *Nature Med.* **4** 861–5
- Boppart S A, Brezinski M E, Pitris C and Fujimoto J G 1998b *Neurosurgery* **43** 834–41
- Boppart S A, Brezinski M E, Tearney G J, Bouma B E and Fujimoto J G 1996 *J. Neurosci. Meth.* **70** 65–72
- Boppart S A, Tearney G J, Bouma B E, Southern J F, Brezinski M E and Fujimoto J G 1997 *Proc. Natl Acad. Sci. USA* **94** 4256–61
- Born M and Wolf E 1980 *Principles of Optics* 6th edn (Oxford: Pergamon)
- Bowd C, Zangwill L, Blumenthal E, Vasile C, Boehm A G, Gokhale P, Mohammadi K, Amini P, Sankary T and Weinreb R 2002 *J. Opt. Soc. Am. A* **19** 199–206
- Brezinski M E and Fujimoto J G 1999 *IEEE J. Select. Topics Quantum Electron.* **5** 1185–92
- Champert P A, Couderc V, Leproux P, Février S, Tombelaïne V, Labonté L, Roy P and Froehly C 2004 *Opt. Express* **12** 4366–71
- Chapeleau X, Leduc D, Wicks M, Ny R L and Boisrobert C 2002 *National Institute of Standard Technological Special Publication* 988, pp 53–6
- Chen Z, Milner T, Dave D and Nelson J 1997 *Opt. Lett.* **22** 64–6
- Chen Z, Milner T, Wang X, Srinivas S and Nelson J 1998 *Photochem. Photobiol.* **67** 56–60
- Chen Z, Zhao Y, Srinivas S M, Nelson J S, Prakash N and Frostig R D 1999 *IEEE J. Select. Topics Quantum Electron.* **5** 1134–42
- Cheong W F, Pahl S A and Welch A J 1990 *IEEE J. Select. Topics Quantum Electron.* **26** 2166–85
- Cheung J Y, Vaughan M P, Mountford J R and Chunnillall C J 2004 *Proc. SPIE* **5161** 365–76
- Chinn S R and Swanson E A 1996 *Opt. Lett.* **21** 899–901
- Chinn S R, Swanson E A and Fujimoto J G 1997 *Opt. Lett.* **22** 340–2
- Choma M A, Sarunic M V, Yang C and Izatt J A 2003 *Opt. Express* **11** 2183–9
- de Boer J, Milner T, van Gemert M and Nelson J S 1997 *Opt. Lett.* **22** 934–6
- de Boer J F, Cense B, Park B H, Pierce M C, Tearney G J and Bouma B E 2003 *Opt. Lett.* **28** 2067–9
- de Boer J F, Srinivas S M, Nelson J S, Milner T E and Ducros M G 2002 *Handbook of Optical Coherence Tomography* ed B E Bouma and G J Tearney (New York: Dekker) pp 237–74
- Derickson D 1998 *Fiber Optic Test and Measurement* (Englewood Cliffs, NJ: Prentice-Hall)
- Dirac P A M 1927 *Proc. R. Soc. A* **114** 243–65
- Drexler W 2004 *J. Biomed. Opt.* **9** 47–71
- Dubois A, Moneron G, Grieve K and Boccara A C 2004 *Phys. Med. Biol.* **49** 1227–34
- Ducros M, Marsack J, III H R, Thomsen S and Milner T 2001 *J. Opt. Soc. Am. A* **18** 2945–56
- Duncan M D, Bashkansky M and Reintjes J 1998 *Opt. Express* **2** 540–5
- Dunkers J P, Cicerone M T and Washburn N R 2003 *Opt. Express* **11** 3074–9
- Dunkers J P, Parnas R S, Zimba C G, Peterson R C, Flynn K M, Fujimoto J G and Bouma B E 1999 *Composites A* **30** 139–45
- Dunkers J P, Phelan F R, Zimba C G, Flynn K M, Saunders D P, Peterson R C and Parnas R S 2001 *Polym. Compos.* **22** 803–14
- Dunsby C and French P M W 2003 *J. Phys. D: Appl. Phys.* **36** R207–27
- Durduran T, Choe R, Culver J P, Zubkov L, Holboke M J, Giammarco J, Chance B and Yodh A G 2002 *Phys. Med. Biol.* **47** 2847–61
- Fantini S, Walker S, Franceschini M, Kaschke M, Schlag P and Moesta K 1998 *Appl. Opt.* **37** 1982–9
- Feldchtein F I, Reitze D, Sergeev A, Gelikonov V, Gelikonov G, Kuranov R, Gladkova N, Iksanov R, Ourutina M and Warren J 1998 *Opt. Express* **3** 239–50
- Feng Y, Wang R K and Elder J B 2003 *J. Opt. Soc. Am. A* **20** 1792–803
- Fercher A F, Drexler W, Hitzinger C K and Lasser T 2003 *Rep. Prog. Phys.* **66** 239–303
- Fercher A F, Hitzinger C K, Kamp G and El-Zaiat S Y 1995 *Opt. Commun.* **43** 43
- Fercher A F, Hitzinger C K, Sticker M, Zawadzki R, Karamata B and Lasser T 2001 *Opt. Express* **9** 610–15
- Fermi E 1932 *Rev. Mod. Phys.* **4** 87–132
- Flournoy P, McClure R and Wyntjes G 1972 *Appl. Opt.* **11**, 1907–15
- Franson J D 1992 *Phys. Rev. A* **45** 3126–32
- Fukana T and Yamaguchi I 1996 *Opt. Lett.* **21** 1942–4
- Ghosh R, Hong C K, Ou Z Y and Mandel L 1986 *Phys. Rev. A* **34** 3962–8
- Ghosh R and Mandel L 1987 *Phys. Rev. Lett.* **59** 1903–5
- Gillis A and Zeyen T 2004 *Bull. Soc. Belge Ophthalmol.* **292** 71–5
- Glauber R J 1963 *Phys. Rev.* **130** 2529–39
- Grant P, Tomlins P, Khurana M, Vadgamma P, James S and Mikhailovsky S 2003 *In-vivo* usage of biomaterials: A snapshot of current activity *NPL Report MATC (A)* 159 National Physical Laboratory, Teddington, England
- Grosenick D, Wabnitz H, Moesta K, Mucke J, Miller M, Stroszczyński C, Stöbel J, Wassermann B, Schlag P and Rinneberg H 2004 *Phys. Med. Biol.* **49** 1165–81
- Hariharan P 2003 *Optical Interferometry* 2nd edn (New York: Academic)

- Haruna M, Ohmi M, Mitsuyama T, Tajiri H, Mayuyama H and Hashimoto M 1998 *Opt. Lett.* **23** 966–8
- Hee M, Huang D, Swanson E and Fujimoto J 1992 *J. Opt. Soc. Am. B* **9** 903–8
- Hee M, Puliafito C, Wong C, Duker J S, Reichel E, Rutledge B, Schuman J S, Swanson E A and Fujimoto J G 1995b *Arch. Ophthalmol.* **113** 1019–2029
- Hee M R, Izatt J A, Swanson E A, Huang D, Schuman J S, Lin C P, Puliafito C A and Fujimoto J G 1995a *Arch. Ophthalmol.* **113** 325–32
- Heffer E and Fantini S 2002 *Appl. Opt.* **41** 3827–39
- Herrmann J, Pitris C, Bouma B, Boppart S, Fujimoto J and Brezinski M 1999 *J. Rheumatol.* **26** 627–63
- Hoeling B M, Fernandez A D, Haskell R C, Huang E, Myers W R, Petersen D C, Ungersma S E, Wang R and Williams M E 2000 *Opt. Express* **6** 136–46
- Hoerauf H and Birngruber R 2002 *Handbook of Optical Coherence Tomography* ed B E Bouma and G J Tearney (New York: Dekker) chapter 18, pp 487–503
- Hong C K, Ou Z Y and Mandel L 1987 *Phys. Rev. Lett.* **59** 2044–6
- Huang D *et al* 1991 *Science* **254** 1178–81
- IEEE Std 1394 1995 *IEEE Standard for a High Performance Serial Bus* Institute of Electrical and Electronics Engineers, New York, USA
- Izatt J A, Hee M R, Owen G M, Swanson E A and Fujimoto J G 1994 *Opt. Lett.* **19** 590–2
- Jackson J D 1999 *Classical Electrodynamics* 3rd edn (New York: Wiley)
- Jerrard H 1982 *Opt. Laser Tech.* **14** 309–19
- Ko T H, Adler D C and Fujimoto J G 2004 *Opt. Express* **12** 2112–19
- Konno S, Akiba J and Yoshida A 2001 *Retina* **21** 57–61
- Kwiat P G, Mattle K, Weinfurter H and Zeilinger A 1995 *Phys. Rev. Lett.* **75** 4337–41
- Lamb W E 1995 *Appl. Phys. B* **60** 77–84
- Legero T, Wilk T, Kuhn A and Rempe G 2003 *Appl. Phys. B* **77** 797–802
- Leitgeb R, Hitznerberger C and Fercher A 2003a *Opt. Express* **11** 889–94
- Leitgeb R, Wojtkowski M, Kowalczyk A, Hitznerberger C, Sticker M and Fercher A 2000 *Opt. Lett.* **25** 820–2
- Leitgeb R A, Schmetterer L, Drexler W, Fercher A F, Zawadzki R J and Bajraszewski T 2003b *Opt. Express* **11** 3116–21
- Leitgeb R A, Schmetterer L, Hitznerberger C K, Fercher A F, Berisha F, Wojtkowski M and Bajraszewski T 2004 *Opt. Lett.* **29** 171–3
- Lexer F, Hitznerberger C, Drexler W, Molebny S, Sattmann H, Sticker M and Fercher A 1999 *J. Mod. Opt.* **46** 541–53
- Li T, Wang A, Murphy K and Claus R 1995 *Opt. Lett.* **20** 785–7
- Li X, Chen J, Voss P, Sharping J and Kumar P 2004 *Opt. Express* **12** 3737–44
- Lin R C, Shure M A, Rollins A M, Izatt J A and Huang D 2004 *Opt. Express* **29** 83–5
- Lindner M, Andretzky P, Kieseewetter F and Häusler G 2002 *Handbook of Optical Coherence Tomography* ed B E Bouma and G J Tearney (New York: Dekker) pp 335–57
- Lissandrin F, Saleh B E A, Sergienko A V and Teich M C 2004 *Phys. Rev. B* **69** 165317–1
- Liu X, Ling Y, Luo R, Ge J and Zheng X 2001 *Chin. Med. J.* **114** 524–9 (Engl. Trans.)
- Loudon R 2000 *The Quantum Theory of Light* 3rd edn (Oxford: Oxford University Press)
- Lozada C J and Altman R D 1999 *Bull. Rheumatic Disease* **46** 5–7
- Lu Q, Gan X, Gu M and Luo Q 2004 *Appl. Opt.* **43** 1628–37
- Mandel L and Wolf E 1995 *Optical Coherence and Quantum Optics* (Cambridge: Cambridge University Press)
- Maruyama H, Inoue S, Mitsuyama T, Ohmi M and Haruna M 2002 *Appl. Opt.* **41** 1315–22
- Mason C, Markusen J F, Town M A, Dunnill P and Wang R K 2004a *Phys. Med. Biol.* **49** 1097–116
- Mason C, Markusen J F, Town M A, He Y, Dunnill P and Wang R K 2004b *Biosensors Bioelectron.* **20** 414–23
- Matcher S J, Cope M and Delpy D T 1997 *Appl. Opt.* **36** 386–96
- Matcher S J, Winlove C P and Gangnus S V 2004 *Phys. Med. Biol.* **49** 1295–306
- Mayhew T A, Williams G R, Senica M A, Kuniholm G and DuMoulin G C 1998 *Tissue Eng.* **4** 325–34
- Morgner U, Drexler W, Kärtner F, Li X, Pitris C, Ippen E and Fujimoto J 2000 *Opt. Lett.* **25** 111–3
- Muscat S, McKay N, Parks S, Kemp E and Keating D 2002 *Invest. Ophthalmol. Vis. Sci.* **43** 1791–5
- Nasr M B, Saleh B E A, Sergienko A V and Teich M C 2003 *Phys. Rev. Lett.* **91** 083601–1
- Nasr M B, Saleh B E A, Sergienko A V and Teich M C 2004 *Opt. Express* **12** 1353–62
- Nassif N, Cense B, Park B H, Yun S H, Chen T C, Bouma B E, Tearney G J and de Boer J F 2004b *Opt. Lett.* **29** 480–2
- Nassif N, Park B, Pierce M, Yun S, Bouma B, Tearney G, Chen T and de Boer J 2004a *Opt. Express* **12** 367–76
- O'Mahony C, Hill M, Brunet M, Duane R and Mathewson A 2003 *Meas. Sci. Technol.* **14** 1807–14
- Otis L L, Colston B W Jr, Everett M J and Nathel H 2000 *Dentomaxillofac. Radiol.* **29** 85–9
- Oxborrow M 2003 *private communication*
- Oxborrow M 2004 *private communication*
- Pan Y, Xie T, Du C, Bastacky S, Meyers S and Zeidel M 2003 *Opt. Lett.* **28** 2485–7
- Pircher M, Gotzinger E, Leitgeb R, Fercher A and Hitznerberger C 2003 *Opt. Express* **11** 2190–7
- Podoleanu A, Charalambous I, Plesea L, Dogariu A and Rosen R 2004 *Phys. Med. Biol.* **49** 1277–94
- Podoleanu A G and Jackson D A 1999 *Appl. Opt.* **38** 2116–27
- Proskurin S G, He Y and Wang R 2004 *Phys. Med. Biol.* **49** 1265–76
- Rao B, Zhang J, Taban M, McDonnell P and Chen Z 2003 *Opt. Express* **11** 3254–61
- Rogowska J, Bryant C and Brezinski M 2003 *J. Opt. Soc. Am. A* **20** 357–67
- Schmitt J, Kolstad D and Petersen C 2004 *Optics Photonics News* **15** (2) 20–5
- Schmitt J, Lee S and Yung K 1997 *Opt. Commun.* **142** 203–7
- Schmitt J M 1999 *IEEE J. Select. Topics Quantum Electron.* **5** 1205–15
- Schmitt J M, Knüttel A and Bonner R F 1993 *Appl. Opt.* **32** 6032–42
- Schmitt J M, Knüttel A, Yadlowsky M and Eckhaus M 1994 *Phys. Med. Biol.* **39** 1705–20
- Schmitt J M and Kumar G 1998 *Appl. Opt.* **37** 2788–97
- Schuman J S, Hee M R, Puliafito C A, Wong C, Pedut-Kloizman T, Lin C P, Hertzmark E, Izatt J A, Swanson E A and Fujimoto J G 1995 *Arch. Ophthalmol.* **113** 586–96
- Sergeev A, Gelikonov V, Gelikonov G, Feldchtein F, Kuranov R and Gladkova N 1997 *Opt. Express* **1** 432–40
- Shih Y 2003 *Rep. Prog. Phys.* **66** 1009–44
- Sivak M V Jr, Kobayashi K, Izatt J, Rollins A, Ungarunyawee R, Chak A, Wong R and Isenberg G 1999 *Gastrointest. Endosc.* **49** AB159
- Smith E D J, Zvyagin A V and Sampson D D 2002 *Opt. Lett.* **27** 1998–2000
- Smithies D J, Lindmo T, Chen Z, Nelson J S and Milner T E 1998 *Phys. Med. Biol.* **43** 3025–44
- Steinberg A M, Kwiat P G and Chiao R Y 1992 *Phys. Rev. Lett.* **68** 2421
- Strasswimmer J, Pierce M C, Park B H, Neel V and de Boer J F 2004 *J. Biomed. Opt.* **9** 292–8
- Swanson E, Izatt J, Hee M, Huang D, Lin C, Schuman J, Puliafito C and Fujimoto J 1993 *Opt. Lett.* **18** 1864–6
- Tearney G, Brezinski M, Bouma B, Boppart S, Pitris C, Southern J and Fujimoto J 1997 *Science* **276** 2037–9
- Thrane L, Frosz M H, Jørgensen T M, Tycho A, Yura H T and Andersen P E 2004 *Opt. Lett.* **29** 1641–3
- Thrane L, Yura H T and Andersen P E 2000 *J. Opt. Soc. Am. A* **17** 484–90
- Tomlins P E, Grant P, Vadgama P, James S and Mikhilovsky S 2004 Structural characterisation of polymer based tissue scaffolds

- NPL Measurement Note DEPC-MN-002 National Physical Laboratory, Teddington, England
- Tomlins P H 2003 Investigation of non-linearity in long fibre amplifiers NPL Report CETM 54 National Physical Laboratory, Teddington, England
- Tripathi R, Nassif N, Nelson J S, Park B H and de Boer J F 2002 *Opt. Lett.* **27** 406–8
- Tseng S H, Greene J H, Tafflove A, Maitland D, Backman V and Walsh J T Jr 2004 *Opt. Lett.* **29** 1393–5
- Tycho A, Jørgensen T M, Yura H T and Andersen P E 2002 *Appl. Opt.* **41** 6676–91
- Unterhuber A *et al* 2003 *Opt. Express* **28** 905–7
- Unterhuber A *et al* 2004 *Phys. Med. Biol.* **49** 1235–46
- Vabre L, Dubois A and Boccara A 2002 *Opt. Lett.* **27** 530–2
- Wang H W, Izatt J A and Kulkarni M D 2002b *Handbook of Optical Coherence Tomography* ed B E Bouma and G J Tearney (New York: Dekker) chapter 10, pp 275–98
- Wang J 2002d *Am. J. Ophthalmol.* **134** 93–8
- Wang J, Fonn D, Simpson T and Jones L 2002e *Am. J. Ophthalmol.* **133** 315–9
- Wang J, Fonn D, Simpson T and Jones L 2003c *Invest. Ophthalmol. Vis. Sci.* **44** 2524–8
- Wang L J, Hong C K and Friberg S R 2001a *J. Opt. B: Quantum Semiclass. Opt.* **3** 346–52
- Wang R K 1999 *J. Mod. Opt.* **46** 1905–12
- Wang R K 2000 *J. Mod. Opt.* **47** 103–20
- Wang R K 2002a *Phys. Med. Biol.* **47** 2281–99
- Wang R K 2004 *Meas. Sci. Technol.* **15** 725–33
- Wang R K and Elder J B 2002c *Lasers Surgery Med.* **30** 201–8
- Wang R K, Tuchin V V, Xu X and Elder J B 2001b *J. Opt. Soc. Am. B* **18** 948–53
- Wang R K, Xu X, He Y and Elder J B 2003b *IEEE J. Select. Topics Quantum Electron.* **9** 234–42
- Wang Y, Nelson J S, Chen Z, Reiser B J, Chuck R S and Windeler R S 2003a *Opt. Express* **11** 1411–7
- Westphal V, Rollins A M, Radhakrishnan S and Izatt J A 2002 *Opt. Express.* **10** 397–404
- Wojtkowski M, Bajraszewski T, Targowski P and Kowalczyk A 2003 *Opt. Lett.* **28** 1745–7
- Xu M, Cai W, Lax M and Alfano R R 2001 *Opt. Lett.* **26** 1066–8
- Yang C, Choma M A, Lamb L E, Simon J D and Izatt J A 2004a *Opt. Lett.* **29** 1396–8
- Yang C, McGuckin L, Simon J, Choma M, Applegate B and Izatt J 2004b *Opt. Lett.* **29** 2016–18
- Yariv A 1985 *Optical Electronics* 3rd edn (New York: Holt, Rinehart and Winston)
- Yasuno Y, Sutoh Y, Nakama M, Makita S, Itoh M, Yatagai T and Mori M 2002 *Opt. Lett.* **27** 403–5
- Yeh P 1988 *Optical Waves in Layered Media* (New York: Wiley)
- Youngquist R C, Carr S and Davies D E N 1987 *Opt. Lett.* **12** 158–60
- Zhao Y, Chen Z, Saxer C, Shen Q, Xiang S, de Boer J F and Nelson J S 2000 *Opt. Lett.* **25** 1358–60
- Zuluaga A F and Richards-Kortum R 1999 *Opt. Lett.* **24** 519–21